

# Symmetry-Protected Majorana Fermions in Topological Crystalline Superconductors: Theory and Application to $\text{Sr}_2\text{RuO}_4$

Yuji Ueno,<sup>1</sup> Ai Yamakage,<sup>1</sup> Yukio Tanaka,<sup>1</sup> and Masatoshi Sato<sup>1,\*</sup>

<sup>1</sup>*Department of Applied Physics, Nagoya University, Nagoya 464-8603, Japan*

(Dated: August 14, 2018)

Crystal point group symmetry is shown to protect Majorana fermions (MFs) in spinfull superconductors (SCs). We elucidate the condition necessary to obtain MFs protected by the point group symmetry. We argue that superconductivity in  $\text{Sr}_2\text{RuO}_4$  hosts a topological phase transition to a topological crystalline SC, which accompanies a  $\mathbf{d}$ -vector rotation under a magnetic field along the  $c$ -axis. Taking all three bands and spin-orbit interactions into account, symmetry-protected MFs in the topological crystalline SC are identified. Detection of such MFs provides evidence of the  $\mathbf{d}$ -vector rotation in  $\text{Sr}_2\text{RuO}_4$  expected from Knight shift measurements but not yet verified.

PACS numbers:

*Introduction* – There has been a recent interest in the realization of Majorana fermions (MFs) in topological superconductors (SCs) [1–3]. While it is known that spin-triplet SCs can host topological superconductivity [4–8], a recent breakthrough indicates that conventional  $s$ -wave superconducting states may also support the topological phase in the presence of spin-orbit interactions [9–13]. The features of  $s$ -wave superconductivity and its possible application to fault-tolerant topological quantum computation have stimulated both theoretical and experimental activities. The  $s$ -wave superconducting scheme has been applied to a wide class of condensed matter systems [14–20].

While these developments are based on topological classifications using the general symmetries of time-reversal and charge conjugation [21], systems often have other symmetries specific to their structures such as translational, rotational, and point group symmetries [22]. Interestingly, additional symmetries can give rise to a nontrivial topology of the bulk wave functions and gapless states on the boundaries [23–27]. Although these specific symmetries are microscopically sensitive to a small disturbance, recent studies of topological crystalline insulators have shown that if the symmetries are preserved on average, then the existence of gapless boundary states is rather robust [28–31]. Therefore, it is expected that the symmetry-protected topological phase can provide an alternative platform for realizing MFs.

In this Letter, we clarify how the crystal point group symmetry may protect the existence of MFs in SCs. We focus here on *spinfull SCs with point group symmetry*. While the time-reversal symmetry may protect MFs in spinful SCs [21, 32, 33], the present theory also works even without the time-reversal invariance. Our arguments are directly applicable to many unconventional SCs, most of which are spinfull.

Using a representation of the gap function for the point group symmetry, we first elucidate the condition necessary to obtain MFs protected by the point group symmetry. We demonstrate that when this condition is satisfied,

spinfull SCs can be separated into a pair of spinless topological SCs, each of which supports MFs. If the conditions are not satisfied, however, the system reduces to a pair of states that are topologically of the same class as quantum Hall states, and thus they only support Dirac fermions at most.

As a concrete example, we apply these arguments to the two-dimensional SC in  $\text{Sr}_2\text{RuO}_4$ . It is argued that  $\text{Sr}_2\text{RuO}_4$  hosts a profound topological phase transition from a chiral topological SC to a topological crystalline SC accompanied by  $\mathbf{d}$ -vector rotation under a magnetic field parallel to the  $c$ -axis. We identify the symmetry-protected MFs by taking all three bands and spin-orbit interactions into account. Detection of the symmetry-protected MFs provides a distinct signature of the  $\mathbf{d}$ -vector rotation in  $\text{Sr}_2\text{RuO}_4$ . Such a rotation is expected from Knight shift measurements but is yet to be verified.

*Symmetry Protected Majorana Fermions* – We first consider two-dimensional SCs, and later discuss the generalization to three-dimensional SCs. We begin with a description of two-dimensional SC based on the Bogoliubov de Gennes (BdG) Hamiltonian  $\mathcal{H} = \sum_{\mathbf{k}} \Psi_{\mathbf{k}}^\dagger \mathcal{H}(\mathbf{k}) \Psi_{\mathbf{k}}/2$ :

$$\mathcal{H}(\mathbf{k}) = \begin{pmatrix} \mathcal{E}(\mathbf{k}) & \Delta(\mathbf{k}) \\ \Delta^\dagger(\mathbf{k}) & -\mathcal{E}^T(-\mathbf{k}) \end{pmatrix}, \Psi_{\mathbf{k}} = (c_{\mathbf{k}sl}, c_{-\mathbf{k}sl}^\dagger)^\dagger, \quad (1)$$

where  $c_{\mathbf{k}sl}$  is the annihilation operator of electrons with momentum  $\mathbf{k} = (k_x, k_y)$  and spin  $s$ ,  $l$  denotes the orbital degrees of freedom of the electron,  $\mathcal{E}(\mathbf{k})$  is the Hamiltonian of the normal state, and  $\Delta(\mathbf{k})$  is the gap function of the SC. Here, the spin ( $s = \uparrow, \downarrow$ ) and orbital ( $l = 1, \dots, N$ ) indices are implicit in  $\mathcal{E}(\mathbf{k})$  and  $\Delta(\mathbf{k})$ . Both  $\mathcal{E}(\mathbf{k})$  and  $\Delta(\mathbf{k})$  are  $2N \times 2N$  matrices. Assuming that the normal state has a mirror symmetry with respect to the  $xy$ -plane as  $\mathcal{M}_{xy} \mathcal{E}(\mathbf{k}) \mathcal{M}_{xy}^\dagger = \mathcal{E}(\mathbf{k})$ , where  $\mathcal{M}_{xy}$  is the unitary matrix of the mirror reflection, we demonstrate how this mirror symmetry ensures topologically stable MFs.

We note that the superconducting state retains the mirror symmetry if the gap function  $\Delta(\mathbf{k})$  is even or odd

under the mirror reflection,  $\mathcal{M}_{xy}\Delta(\mathbf{k})\mathcal{M}_{xy}^\dagger = \pm\Delta(\mathbf{k})$ . In the former (latter) case,  $\mathcal{H}(\mathbf{k})$  is invariant under the mirror reflection

$$\tilde{\mathcal{M}}_{xy}\mathcal{H}(\mathbf{k})\tilde{\mathcal{M}}_{xy}^\dagger = \mathcal{H}(\mathbf{k}), \quad (2)$$

with  $\tilde{\mathcal{M}}_{xy} = \tilde{\mathcal{M}}_{xy}^+$  ( $\tilde{\mathcal{M}}_{xy}^-$ ) given by,

$$\tilde{\mathcal{M}}_{xy}^\pm = \begin{pmatrix} \mathcal{M}_{xy} & 0 \\ 0 & \pm\mathcal{M}_{xy}^* \end{pmatrix}. \quad (3)$$

In both these cases,  $\mathcal{H}(\mathbf{k})$  commutes with either of  $\tilde{\mathcal{M}}_{xy}^\pm$  (which we refer to simply as  $\tilde{\mathcal{M}}_{xy}$  in the following). Therefore,  $\mathcal{H}(\mathbf{k})$  is block diagonal in the diagonal basis of  $\tilde{\mathcal{M}}_{xy}$ . Each block-diagonal subsector has a definite eigenvalue of the matrix  $\tilde{\mathcal{M}}_{xy}$ .

The mirror Chern number  $\nu(\lambda)$  is defined as a Chern number of the subsector; using the negative energy states  $|u_n^\lambda(\mathbf{k})\rangle$  in the subsector with the eigenvalue  $\lambda$  of  $\tilde{\mathcal{M}}_{xy}$ , the gauge field in the momentum space is introduced as  $\mathcal{A}_a^\lambda(\mathbf{k}) = i\sum_{E_n < 0} \langle u_n^\lambda(\mathbf{k}) | \partial_{k_a} u_n^\lambda(\mathbf{k}) \rangle$ . The mirror Chern number is then given by

$$\nu(\lambda) = \frac{1}{2\pi} \int_{-\pi}^{\pi} \int_{-\pi}^{\pi} dk_x dk_y \mathcal{F}^\lambda, \quad (4)$$

where  $\mathcal{F}^\lambda$  is the field strength of  $\mathcal{A}_a^\lambda$ , and the integration is performed over the first Brillouin zone,  $-\pi \leq k_{x,y} \leq \pi$ .

The mirror Chern number introduced here is a natural generalization of that used to characterize topological crystalline insulators [23]. Therefore, as well as topological crystalline insulators, the mirror Chern number ensures the existence of gapless boundary states as long as the mirror symmetry is preserved macroscopically. However, as we show, there is an important difference: to stabilize the MFs using the mirror symmetry, an additional requirement for  $\tilde{\mathcal{M}}_{xy}$  is needed.

This additional requirement originates from the symmetry specific to SCs. Because of the self-conjugate property of the quasiparticle field  $\Psi_{\mathbf{k}}$  in Eq. (1),

$$\Psi_{\mathbf{k}} = \mathcal{C}\Psi_{-\mathbf{k}}^*, \quad \mathcal{C} = \begin{pmatrix} 0 & 1 \\ 1 & 0 \end{pmatrix}, \quad (5)$$

the BdG Hamiltonian has the special symmetry  $\mathcal{C}\mathcal{H}(\mathbf{k})\mathcal{C}^\dagger = -\mathcal{H}^*(-\mathbf{k})$ ; i.e., particle-hole symmetry. The self-conjugate property of the particle-hole symmetry is the origin of the Majorana nature of topologically protected gapless states. Therefore, to obtain MFs in a subsector of the system, particle-hole symmetry, which is closed in the subsector, is essential. A subsector of  $\mathcal{H}(\mathbf{k})$  with a definite eigenvalue of  $\tilde{\mathcal{M}}_{xy}$ , however, does not always have particle-hole symmetry within the subsector because this symmetry can exchange a pair of subsectors with different eigenvalues. Thus, only subsectors with particle-hole symmetry can support MFs that are protected by the mirror symmetry.

We now elucidate the condition for a subsector with an eigenvalue  $\lambda$  of  $\tilde{\mathcal{M}}_{xy}$  to host its own particle-hole symmetry. Since the particle-hole symmetry maps a state  $|u(\mathbf{k})\rangle$  with the eigenvalue  $\lambda$  to  $\mathcal{C}|u^*(-\mathbf{k})\rangle$ , the condition is derived so that the mapped state  $\mathcal{C}|u^*(-\mathbf{k})\rangle$  has the same eigenvalue  $\lambda$  as the original one. We find that this leads to

$$\mathcal{C}\tilde{\mathcal{M}}_{xy}\mathcal{C}^\dagger = \lambda^2\tilde{\mathcal{M}}_{xy}^*. \quad (6)$$

In other words, only for  $\tilde{\mathcal{M}}_{xy}$  satisfying Eq. (6) one can obtain MFs protected by the mirror symmetry.

Among the two possible mirror symmetries  $\tilde{\mathcal{M}}_{xy}^\pm$  in Eq. (3), only  $\tilde{\mathcal{M}}_{xy}^-$  satisfies Eq. (6). Indeed, from  $\mathcal{M}_{xy}^2 = -1 = \lambda^2$ , one can show that  $\lambda = \pm i$  and  $\mathcal{C}\tilde{\mathcal{M}}_{xy}^\pm\mathcal{C}^\dagger = \mp\lambda^2\tilde{\mathcal{M}}_{xy}^*$ . These are consistent with Eq. (6) only for  $\tilde{\mathcal{M}}_{xy}^-$ , which means that when the gap function is odd under the mirror reflection  $\mathcal{M}_{xy}\Delta(\mathbf{k})\mathcal{M}_{xy}^\dagger = -\Delta(\mathbf{k})$ , the subsector with the eigenvalue  $\lambda$  supports its own particle-hole symmetry [Fig. 1(a)]. However, when the gap function is even under the mirror reflection  $\mathcal{M}_{xy}\Delta(\mathbf{k})\mathcal{M}_{xy}^\dagger = \Delta(\mathbf{k})$ , the particle-hole symmetry of the original Hamiltonian merely interchanges two different subsectors, and thus each subsector does not have particle-hole symmetry [Fig. 1(b)].

In the latter case, we find that the subsectors belong to class A of the topological classification [21] since there is no particle-hole symmetry. That is, they are topologically the same as quantum Hall states, which also belong to class A [34]. Therefore, even when there are topologically protected states ensured by the mirror Chern number, these states reduce to Dirac fermions as is the case for quantum Hall states.

In contrast, MFs can be realized in the former case: each subsector belongs to class D of the topological classification [21] because of its own particle-hole symmetry. Consequently, as a class D topological phase, the mirror subsector can host MFs. The topological invariant for class D is 0 for three dimensions,  $\mathbf{Z}$  for two dimensions, and  $\mathbf{Z}_2$  for one dimension. Therefore, in addition to the mirror Chern number  $\nu(\lambda)$ , we can define the one-dimensional (1D)  $\mathbf{Z}_2$  invariants  $\nu_x(\lambda)$  and  $\nu_y(\lambda)$  as [7]

$$\nu_x(\lambda) = \frac{1}{\pi} \int_{-\pi}^{\pi} dk_y \mathcal{A}_y^\lambda(\pi, k_y) \pmod{2}, \quad (7)$$

which we refer to as mirror  $\mathbf{Z}_2$  invariants ( $\nu_y(\lambda)$  is defined in a similar manner). The 1D mirror  $\mathbf{Z}_2$  invariants are well defined even for a system without time-reversal invariance, and thus they are very different from the  $\mathbf{Z}_2$  invariants for topological (crystalline) insulators.

The topological invariants  $\nu(\lambda)$ ,  $\nu_x(\lambda)$ , and  $\nu_y(\lambda)$  characterize the MFs in the mirror subsector; the mirror Chern number ensures the existence of chiral edge MFs in the mirror subsector. Using a similar argument to that given in Refs. [35] and [36], we can also show that

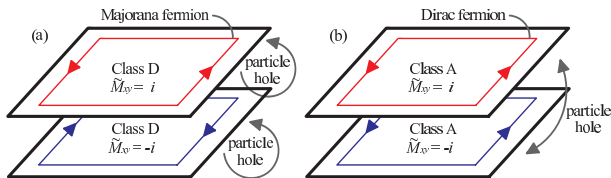


FIG. 1: Two possible realizations of particle-hole symmetry.

if the mirror Chern number is odd, then the Majorana zero-energy states exist on a vortex. Furthermore, the 1D mirror  $\mathbf{Z}_2$  invariants guarantee the existence of Majorana zero-energy bound states localized on a dislocation, if the Burgers vector  $\mathbf{B}$  characterizing the dislocation satisfies  $\mathbf{B} \cdot \mathbf{G}^\lambda = 1 \pmod{2}$  [37]. Here,  $\mathbf{G}^\lambda = \frac{1}{2\pi}(\nu_x(\lambda)\mathbf{b}_x + \nu_y(\lambda)\mathbf{b}_y)$  with  $\mathbf{b}_x$  and  $\mathbf{b}_y$  being the reciprocal lattice vectors in the  $x$ - and  $y$ -directions. All these MFs are topologically stable so long as the mirror symmetry is preserved macroscopically beyond the scale of the coherence length.

A generalization of these results to three-dimensional SCs is fairly straightforward. In three dimensions, Eq. (2) is replaced with  $\tilde{\mathcal{M}}_{xy}\mathcal{H}(k_x, k_y, k_z)\tilde{\mathcal{M}}_{xy}^\dagger = \mathcal{H}(k_x, k_y, -k_z)$ . If we then consider the mirror invariant  $k_x k_y$ -planes with  $k_z = 0$  or  $\pi$ , the same argument as per the two-dimensional case applies, and again symmetry-protected MFs can be realized when the gap function is odd under the mirror reflection. We can also generalize our arguments to other point group symmetries. For instance, like topological crystalline insulators, we can introduce topological invariants using discrete rotation symmetries, but to stabilize the MFs, additional requirements similar to those in Eq. (6) are needed.

*Application to Sr<sub>2</sub>RuO<sub>4</sub>*— To illustrate the general arguments above, we apply our results to the two-dimensional spin-triplet SC Sr<sub>2</sub>RuO<sub>4</sub> [38, 39]. Sr<sub>2</sub>RuO<sub>4</sub> has a tetragonal structure with the crystal point group symmetry  $D_{4h}$  and, in particular, is invariant under a mirror reflection with respect to the  $xy$ -plane. We consider the superconducting state of Sr<sub>2</sub>RuO<sub>4</sub> under magnetic fields in the  $z$ -direction. In this case, the crystal point group symmetry reduces to  $C_{4h}$ , but the system is still invariant under the mirror reflection  $\mathcal{M}_{xy}$ . According to the representation theory of  $C_{4h}$ , the possible spin-triplet gap functions are classified as in Table I.

For zero or weak magnetic fields, a number of experiments support time-reversal breaking chiral  $p_x + ip_y$  superconductivity in Sr<sub>2</sub>RuO<sub>4</sub>, which belongs to the  $E_u$  representation in Table I [38, 39]. The  $\mathbf{d}$ -vector is aligned along the  $z$ -direction, and the gap function,  $\Delta(\mathbf{k}) = i\mathbf{d}(\mathbf{k}) \cdot \boldsymbol{\sigma}\sigma_y$ , is even under the mirror reflection. For magnetic fields greater than 20 mT, Knight shift measurements suggest that the  $\mathbf{d}$ -vector is parallel to the  $xy$ -plane, consistent with the  $A_u$  or  $B_u$  representation in Table I [40]. Thus, the gap function is helical and odd under the mirror reflection. For consistency with both experimental results, there should be a phase transition

TABLE I: Possible  $\mathbf{d}$ -vector states of Sr<sub>2</sub>RuO<sub>4</sub> under magnetic fields in the  $z$ -direction. The representation  $\Gamma$ ,  $\mathbf{d}$ -vector, parity of the gap function  $\Delta = i\mathbf{d} \cdot \boldsymbol{\sigma}\sigma_y$  under the mirror reflection  $\mathcal{M}_{xy}$ , topological class of the subsector with a definite eigenvalue of  $\tilde{\mathcal{M}}_{xy}$ , and mirror topological numbers  $\nu$ ,  $\nu_x$ , and  $\nu_y$  are summarized. Note that the mirror  $\mathbf{Z}_2$  numbers are not defined in the  $E_u$  representation.

$\Gamma$	$\mathbf{d}$ -vector	$\mathcal{M}_{xy}$	subsector	$[\nu(\lambda), \nu_x(\lambda), \nu_y(\lambda)]$
$A_u$	$\hat{x} \sin k_x + \hat{y} \sin k_y$	odd	class D	$[\pm 1, 1, 1]_{\lambda=\pm i}$
$B_u$	$\hat{x} \sin k_x - \hat{y} \sin k_y$	odd	class D	$[\mp 1, 1, 1]_{\lambda=\pm i}$
$E_u$	$\hat{z}(\sin k_x + i \sin k_y)$	even	class A	$[1, -, -]_{\lambda=\pm i}$

at a critical magnetic field  $H_{zc}$  at which the  $\mathbf{d}$ -vector rotates from the  $z$ -direction to the  $xy$ -plane, the chiral superconducting state becomes helical, and the mirror parity of the gap function changes from even to odd.

It is known that the chiral  $p_x + ip_y$  superconducting state in the low-field phase hosts topological superconductivity [41, 42]. Taking the spin degrees of freedom into account, the Chern number of this state is evaluated as  $\nu_{\text{Ch}} = 2$ , and thus a pair of topologically protected chiral fermions exist on the boundary [43–49]. However, our argument implies that it is impossible to detect their Majorana character if  $\mathbf{d} \parallel \hat{z}$ . Since the gap function is even under the mirror reflection, this state can be separated into a pair of subsectors belonging to class A. In each subsector, the paired MFs,  $\gamma_1$  and  $\gamma_2$ , are recast into a single Dirac fermion  $\psi = \gamma_1 + i\gamma_2$ , and thus their dynamics are reduced to those of the Dirac fermion.

In contrast, the helical superconducting state in the high-field phase supports MFs. The ordinary Chern number  $\nu_{\text{Ch}}$  is found to be zero in this phase, and so this phase is not topological in terms of the topological periodic table [21]. Nevertheless, since the gap function is odd under the mirror reflection, the mirror Chern number and the 1D mirror  $\mathbf{Z}_2$  invariants can be introduced. Using a standard adiabatic deformation method for the Hamiltonian, the mirror topological invariants can be calculated, and we find that they are nonzero. The obtained results are summarized in Table I. (For details, see Sec.S2 in Supplementary Material.) From the bulk–boundary correspondence, one can conclude that MFs protected by the mirror symmetry exist. Since the mirror symmetry is essential for hosting the topological phase, the high-field phase realizes a topological crystalline SC[50].

To illustrate these results, we examine the quasiparticle states of Sr<sub>2</sub>RuO<sub>4</sub> using the following model Hamiltonian on the square lattice [51]. The conduction bands of Sr<sub>2</sub>RuO<sub>4</sub> consist of three  $4d-t_{2g}$  Ru orbitals,  $d_{xz}$ ,  $d_{yz}$ , and  $d_{xy}$ , which we label as  $l = 1, 2$ , and 3, respectively. The superconducting state of Sr<sub>2</sub>RuO<sub>4</sub> is described by

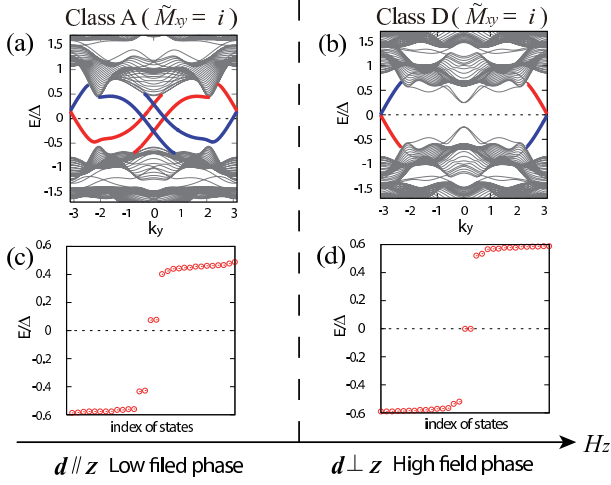


FIG. 2: Topological gapless states in the low- and high-field phases of  $\text{Sr}_2\text{RuO}_4$ . (a) and (b) Edge states and (c) and (d) bound states of the edge dislocation. In (a) and (b), the red (blue) lines represent edge states localized at  $x = 0$  ( $x = L$ ). Results are shown for the  $\tilde{M}_{xy} = i$  sector. The  $\mathbf{d}$ -vector is chosen as  $\mathbf{d}(\mathbf{k}) = \hat{z}(\sin k_x + i \sin k_y)$  in the low-field phase and as  $\mathbf{d}(\mathbf{k}) = \hat{x} \sin k_y - \hat{y} \sin k_x$  in the high-field phase. We take  $t_1 = t_2 = 0.5$ ,  $t_3 = 0.2$ ,  $t_4 = 0.1$ ,  $\mu = -0.2$ ,  $\mu' = -0.2$ ,  $\mu_B H_z = 0.1$ ,  $\lambda = 0.3$ , and  $\Delta^l = 0.6$ .

the BdG Hamiltonian  $\mathcal{H} = \mathcal{H}_{\text{kin}} + \mathcal{H}_{\text{so}} + \mathcal{H}_{\text{pair}}$ , in which

$$\begin{aligned} \mathcal{H}_{\text{kin}} &= \sum_{\mathbf{k}s} (c_{\mathbf{k}s1}^\dagger, c_{\mathbf{k}s2}^\dagger, c_{\mathbf{k}s3}^\dagger) \begin{pmatrix} \varepsilon_{\mathbf{k}1} & g_{\mathbf{k}} & 0 \\ g_{\mathbf{k}} & \varepsilon_{\mathbf{k}2} & 0 \\ 0 & 0 & \varepsilon_{\mathbf{k}3} \end{pmatrix} \begin{pmatrix} c_{\mathbf{k}s1} \\ c_{\mathbf{k}s2} \\ c_{\mathbf{k}s3} \end{pmatrix}, \\ \mathcal{H}_{\text{so}} &= i\lambda \sum_{lmn} \epsilon_{lmn} \sum_{\mathbf{k}ss'} c_{\mathbf{k}sl}^\dagger c_{\mathbf{k}s'm} \sigma_{ss'}^n, \\ \mathcal{H}_{\text{pair}} &= \frac{1}{2} \sum_{klss'} \hat{\Delta}_{ss'}^l(\mathbf{k}) c_{\mathbf{k}sl}^\dagger c_{-\mathbf{k}s'l}^\dagger + \text{h.c.} \end{aligned} \quad (8)$$

where  $\varepsilon_{\mathbf{k}1} = -2t_1 \cos k_y - \mu$ ,  $\varepsilon_{\mathbf{k}2} = -2t_1 \cos k_x - \mu$ , and  $\varepsilon_{\mathbf{k}3} = -2t_2(\cos k_x + \cos k_y) - 4t_3 \cos k_x \cos k_y - \mu'$  are the kinetic terms of orbital 1, 2, and 3, respectively,  $g_{\mathbf{k}} = -4t_4 \sin k_x \sin k_y$  is the hybridization of orbital 1 and 2, and  $\hat{\Delta}^l(\mathbf{k}) = i\Delta^l \mathbf{d}(\mathbf{k}) \cdot \boldsymbol{\sigma} \sigma_y$  is the gap function with  $\mathbf{d}(\mathbf{k})$  as defined in Table I. Here,  $\sigma^n$  is the Pauli matrix, and  $\epsilon_{lmn}$  is the completely antisymmetric tensor. In the  $(c_{\mathbf{k}s1}, c_{\mathbf{k}s2}, c_{\mathbf{k}s3})$  basis,  $\mathcal{M}_{xy}$  is given by  $\mathcal{M}_{xy} = \text{diag}(-i\sigma_z, -i\sigma_z, i\sigma_z)$ . For definiteness, we assume  $\mathbf{d}(\mathbf{k}) = \hat{x} \sin k_y - \hat{y} \sin k_x$  in the high-field phase, but a qualitatively similar result is obtained as long as the  $\mathbf{d}$ -vector is parallel to the  $xy$ -plane.

To examine the edge states of  $\text{Sr}_2\text{RuO}_4$ , we numerically diagonalize the BdG Hamiltonian Eq. (8) in the coordinate space with open boundaries at  $x = 0$  and  $x = L = 30$ . Using the mirror symmetry, we separate the quasiparticle spectra into two subsectors with different eigenvalues of  $\tilde{M}_{xy}$ . Figures 2(a) and (b) illustrate the quasiparticle spectra in the  $\tilde{M}_{xy} = i$  sector. A similar result is obtained in the  $\tilde{M}_{xy} = -i$  sector. Gapless

edge states for both the low-field phase [Fig. 2 (a)] and the high-field phase [Fig. 2 (b)] can be seen clearly, which is consistent with the nonzero mirror Chern numbers in both phases. The degeneracy of these edge states at  $k_y = 0$  [43–47] is resolved by the multi-orbital spin-orbit interaction. Note, however, that there is an essential difference between the two phases. While the quasiparticle spectrum in the high-field phase is particle–hole symmetric as  $E(k_y) = -E(-k_y)$ , that in the low-field phase is not. This indicates clearly that only the high-field phase supports edge MFs. Note also that the particle–hole symmetry in the low-field phase is recovered if it is considered in conjunction with the  $\tilde{M}_{xy} = -i$  sector.

Here we would like to mention that the existence of gapless states in Fig.2 (b) is consistent with the Ising behavior of helical MFs [52–55]: Helical MFs remain gapless except under a magnetic field along a special direction determined by the  $\mathbf{d}$ -vector. As well as Ref.[56], the present result reveals that symmetry protection is essential for the Majorana Ising character.

The bound states of the edge dislocations are shown in Figs. 2(c) and (d). The energy spectra were calculated on  $30 \times 30$  unit cell system with periodic boundary conditions in the  $x$ - and  $y$ -directions. Two edge dislocations with the Burgers vector  $\mathbf{B} = \pm \hat{e}_x$ , separated by half the length of the system size, are considered. (See Sec.S3 in Supplementary Material.) In the high-field phase, we have  $\mathbf{G}^\lambda = \frac{1}{2\pi}(\mathbf{b}_x + \mathbf{b}_y)$  from Table I, so  $\mathbf{G}^\lambda \cdot \mathbf{B} = 1$ , which predicts the existence of a zero mode in the dislocation. The high-field phase can be seen to support zero energy states, which are localized on the edge dislocations and are two-fold degenerate because there are two dislocations in the system. Therefore, there is a single Majorana zero mode localized on each edge dislocation.

In the same way as ordinary MFs, these symmetry-protected MFs can be identified by tunneling spectroscopy. In particular, the detection of the zero mode in the dislocation gives a strong signature of the  $\mathbf{d}$ -vector rotation in the high-field phase; if the  $\mathbf{d}$ -vector rotation does not occur, the bound state in the dislocation must have a gap of  $O(\mu_B H_z)$ . Thus, the observation of the zero energy state is a distinct signal of the  $\mathbf{d}$ -vector rotation. The change in the edge-mode spectra can also provide details of the tunneling conductance. In addition, in each sector of a definite eigenvalue of  $\tilde{M}_{xy}$ , the symmetry-protected MFs behave like ordinary MFs and retain the unique features specific to MFs [57–64].

*Discussions* – The symmetry-protected MFs discussed here are applicable to many unconventional SC; the same arguments apply equally to  $\text{Cu}_x\text{Bi}_2\text{Se}_3$  [8, 65–69] and  $\text{UPt}_3$  [70, 71] as both these crystals have a mirror plane. Details about these systems will be reported elsewhere.

The authors are grateful to S. Kashiwaya for fruitful discussions. This work was supported by the JSPS (Nos. 2074023303, 2134010303, and 22540383) and KAKENHI Grants-in-Aid (Nos. 22103002 and 22103005) from

MEXT.

- 
- \* Electronic address: msato@nuap.nagoya-u.ac.jp
- [1] Y. Tanaka, M. Sato, and N. Nagaosa, *J. Phys. Soc. Jpn.* **81**, 011013 (2012).
- [2] X.-L. Qi and S.-C. Zhang, *Rev. Mod. Phys.* **83**, 1057 (2011).
- [3] F. Wilczek, *Nature Phys.* **5**, 614 (2009).
- [4] N. Reed and D. Green, *Phys. Rev. B* **61**, 10267 (2000).
- [5] D. A. Ivanov, *Phys. Rev. Lett.* **86**, 268 (2001).
- [6] M. Sato, *Phys. Rev. B* **79**, 214526 (2009).
- [7] M. Sato, *Phys. Rev. B* **81**, 220504(R) (2010).
- [8] L. Fu and E. Berg, *Phys. Rev. Lett.* **105**, 097001 (2010).
- [9] M. Sato, *Phys. Lett. B* **575**, 126 (2003).
- [10] L. Fu and C. L. Kane, *Phys. Rev. Lett.* **100**, 096407 (2008).
- [11] M. Sato, Y. Takahashi, and S. Fujimoto, *Phys. Rev. Lett.* **103**, 020401 (2009).
- [12] J. D. Sau, R. M. Lutchyn, S. Tewari, and S. D. Sarma, *Phys. Rev. Lett.* **104**, 040502 (2010).
- [13] J. Alicea, *Phys. Rev. B* **81**, 125318 (2010).
- [14] M. Sato, Y. Takahashi, and S. Fujimoto, *Phys. Rev. B* **82**, 134521 (2010).
- [15] X.-J. Liu and H. Hu, *Phys. Rev. A* **85**, 033622 (2012).
- [16] R. Wei and E. Mueller, *Phys. Rev. A* **86**, 063604 (2012).
- [17] H. Zhai, *Int. J. Mod. Phys. B* **26**, 1230001 (2012).
- [18] R. M. Lutchyn, J. D. Sau, and S. Das Sarma, *Phys. Rev. Lett.* **105**, 077001 (2010).
- [19] Y. Oreg, G. Refael, and F. von Oppen, *Phys. Rev. Lett.* **105**, 177002 (2010).
- [20] J. Alicea, Y. Oreg, G. Refael, F. von Oppen, and M. P. A. Fisher, *Nat. Phys.* **7**, 412 (2011).
- [21] A. P. Schnyder, S. Ryu, A. Furusaki, and A. W. W. Ludwig, *Phys. Rev. B* **78**, 195125 (2008).
- [22] N. W. Ashcroft and N. D. Mermin, *Solid State Physics* (Saunders College Publishing, 1976).
- [23] L. Fu, *Phys. Rev. Lett.* **106**, 106802 (2011).
- [24] T. L. Hughes, E. Prodan, and B. A. Bernevig, *Phys. Rev. B* **83**, 245132 (2011).
- [25] A. M. Turner, Y. Zhang, and A. Vishwanath, *Phys. Rev. B* **82**, 241102(R) (2010).
- [26] T. Hsieh, H. Lin, J. Liu, W. Duan, A. Bansil, and L. Fu (2012).
- [27] R.-J. Slager, A. Mesaros, V. Juricic, and J. Zaanen, *Nature Physics* **9**, 98 (2013).
- [28] Z. Ringel, Y. E. Kraus, and A. Stern, *Phys. Rev. B* **86**, 045102 (2012).
- [29] R. S. K. Mong, J. Bardarson, and J. E. Moore, *Phys. Rev. Lett.* **108**, 076804 (2012).
- [30] L. Fu and C. L. Kane, *Phys. Rev. Lett.* **109**, 246605 (2012).
- [31] I. C. Fulga, B. van Heck, J. M. Edge, and A. R. Akhmerov, arXiv:1212.6191.
- [32] X. L. Qi, T. L. Hughes, S. Raghu, and S. C. Zhang, *Phys. Rev. Lett.* **102**, 187001 (2009).
- [33] R. Roy, arXiv:0803.2863.
- [34] This does not imply the time-reversal breaking of the gap function while the time-reversal symmetry is broken in the quantum Hall state. Because the time-reversal operation flips the spin, the mirror subsector does not have the time-reversal symmetry even if the whole system is time-reversal invariant.
- [35] R. Roy, *Phys. Rev. Lett.* **105**, 186401 (2010).
- [36] J. C. Y. Teo and C. L. Kane, *Phys. Rev. B* **82**, 115120 (2010).
- [37] D. Asahi and N. Nagaosa, *Phys. Rev. B* **86**, 100504(R) (2012).
- [38] A. P. Mackenzie and Y. Maeno, *Rev. Mod. Phys.* **75**, 657 (2003).
- [39] Y. Maeno, S. Kitaoka, T. Nomura, S. Yonezawa, and K. Ishida, *J. Phys. Soc. Jpn.* **81**, 011009 (2012).
- [40] H. Murakawa, K. Ishida, K. Kitagawa, Z. Q. Mao, and Y. Maeno, *Phys. Rev. Lett.* **93**, 167004 (2004).
- [41] G. E. Volovik, *JETP Lett.* **66**, 522 (1997).
- [42] J. Goryo and K. Ishikawa, *J. Phys. Soc. Jpn.* **67**, 3006 (1998).
- [43] M. Yamashiro, Y. Tanaka, and S. Kashiwaya, *Phys. Rev. B* **56**, 7847 (1997).
- [44] C. Honerkamp and M. Sigrist, *J. Low Temp. Phys.* **111**, 895 (1998).
- [45] M. Matsumoto and M. Sigrist, *J. Phys. Soc. Jpn.* **68**, 994 (1999).
- [46] A. Furusaki, M. Matsumoto, and M. Sigrist, *Phys. Rev. B* **64**, 054514 (2001).
- [47] K. Sengupta, H.-J. Kwon, and V. M. Yakovenko, *Phys. Rev. B* **65**, 104504 (2002).
- [48] S. Kashiwaya, H. Kashiwata, H. Kambara, T. Furuta, H. Yaguchi, Y. Tanaka, and Y. Maeno, *Phys. Rev. Lett.* **107**, 077003 (2011).
- [49] Y. Imai, K. Wakabayashi, and M. Sigrist, *Phys. Rev. B* **85**, 174532 (2012).
- [50] J. C. Y. Teo and T. L. Hughes, arXiv:1208.6303.
- [51] K. K. Ng and M. Sigrist, *Europhys. Lett.* **49**, 473 (2000).
- [52] M. Sato and S. Fujimoto, *Phys. Rev. B* **79**, 094504 (2009).
- [53] S.-B. Chung and S.-C. Zhang, *Phys. Rev. Lett.* **103**, 225301 (2009).
- [54] G. E. Volovik, *JETP Lett.* **91**, 201 (2010).
- [55] R. Shindou, A. Furusaki, and N. Nagaosa, *Phys. Rev. B* **82**, 180505(R) (2010).
- [56] T. Mizushima, M. Sato, and K. Machida, *Phys. Rev. Lett.* **109**, 165301 (2012).
- [57] C. J. Bolech and E. Demler, *Phys. Rev. Lett.* **98**, 237002 (2007).
- [58] J. Nilsson, A. R. Akhmerov, and C. W. J. Beenakker, *Phys. Rev. Lett.* **101**, 120403 (2008).
- [59] A. R. Akhmerov, J. Nilsson, and C. W. J. Beenakker, *Phys. Rev. Lett.* **102**, 216404 (2009).
- [60] K. T. Law, P. A. Lee, and T. K. Ng, *Phys. Rev. Lett.* **103**, 237001 (2009).
- [61] Y. Tanaka, T. Yokoyama, and N. Nagaosa, *Phys. Rev. Lett.* **103**, 107002 (2009).
- [62] J. Linder, Y. Tanaka, T. Yokoyama, A. Sudbo, and N. Nagaosa, *Phys. Rev. Lett.* **104**, 067001 (2010).
- [63] J. Alicea, *Rep. Prog. Phys.* **75**, 076501 (2012).
- [64] C. W. J. Beenakker, arXiv:1112.1950.
- [65] Y. S. Hor, A. J. Williams, J. G. Checkelsky, P. Roushan, J. Seo, Q. Xu, H. Zandbergen, A. Yazdani, N. P. Ong, and R. J. Cava, *Phys. Rev. Lett.* **104**, 057001 (2010).
- [66] L. A. Wray, S.-Y. Xu, Y. Xia, Y. S. Hor, D. Qian, A.V.Fedorov, H. Lin, A. Bansil, R. J. Cava, and M. Z. Hasan, *Nature Phys.* **6**, 855 (2010).
- [67] S. Sasaki, M. Kriener, K. Segawa, K. Yada, Y. Tanaka, M. Sato, and Y. Ando, *Phys. Rev. Lett.* p. 217001 (2011).

- [68] A. Yamakage, K. Yada, M. Sato, and Y. Tanaka, Phys. Rev. B **85**, 180509 (2012).
- [69] T. H. Hsieh and L. Fu, Phys. Rev. Lett. **108**, 107005 (2012).
- [70] R. Joynt and L. Taillefer, Rev. Mod. Phys. **74**, 235 (2002).
- [71] Y. Machida, A. Itoh, Y. So, K. Izawa, Y. Haga, E. Yamamoto, N. Kimura, Y. Onuki, Y. Tsutsumi, and K. Machida, Phys. Rev. Lett. **108**, 157002 (2012).

## Supplementary Material

### S1. Parity of the gap function under the mirror reflection $\mathcal{M}_{xy}$

Under the mirror reflection with respect to the  $xy$ -plane, the gap function transforms as

$$\hat{\Delta}(\mathbf{k}) \rightarrow \mathcal{M}_{xy} \hat{\Delta}(k_x, k_y, -k_z) \mathcal{M}_{xy}^t, \quad (\text{S.1})$$

with  $\mathbf{k} = (k_x, k_y, k_z)$  and  $\mathcal{M}_{xy} = \pm i\sigma_z$ . If the gap function satisfies  $\mathcal{M}_{xy} \hat{\Delta}(k_x, k_y, -k_z) \mathcal{M}_{xy}^t = \hat{\Delta}(\mathbf{k})$  ( $\mathcal{M}_{xy} \hat{\Delta}(k_x, k_y, -k_z) \mathcal{M}_{xy}^t = -\hat{\Delta}(\mathbf{k})$ ), the parity of the gap function under the mirror reflection is even (odd). In general, the mirror parity is determined completely by the representation of the gap function under the point group symmetry.

For example, consider a gap function that belongs to the trivial representation of an  $s$ -wave gap function  $\hat{\Delta}_s(\mathbf{k}) = i\psi\sigma_y$ . In this case, Eq.(S.1) leads  $\mathcal{M}_{xy} \hat{\Delta}_s(k_x, k_y, -k_z) \mathcal{M}_{xy}^t = \hat{\Delta}_s(\mathbf{k})$ , which implies that the mirror parity of the gap function in the trivial representation is always even.

For a two dimensional spin-triplet gap function  $\hat{\Delta}(\mathbf{k}) = i\mathbf{d}(\mathbf{k})\sigma\sigma_y$  with  $\mathbf{k} = (k_x, k_y)$ , we can relate the mirror parity to the orientation of the  $\mathbf{d}$ -vector. In this case, the right hand side of Eq.(S.1) becomes

$$-id_x(k_x, k_y)\sigma_x\sigma_y - id_y(k_x, k_y)\sigma_y\sigma_y + id_z(k_x, k_y)\sigma_z\sigma_y, \quad (\text{S.2})$$

and thus if the  $\mathbf{d}$ -vector is normal (parallel) to the  $z$ -direction, the mirror parity is odd (even), and vice versa. Therefore, for a two dimensional spin-triplet superconductor like  $\text{Sr}_2\text{RuO}_4$ , the mirror parity is determined by the orientation of the  $\mathbf{d}$ -vector and does not depend on other details of the gap function.

### S2. Mirror topological numbers of $\text{Sr}_2\text{RuO}_4$

In this section, we calculate the mirror topological numbers of  $\text{Sr}_2\text{RuO}_4$ . To calculate the mirror topological numbers, we adiabatically turn off the spin-orbit interaction  $\lambda$  and the inter-orbit hopping  $t_4$  of the Hamiltonian Eq.(8) without gap closing, by changing other parameters of the Hamiltonian slightly if necessary. This process does not change the mirror topological numbers since they can change only when the gap closes. In the absence of the spin-orbit interaction and the inter-orbit coupling, the three orbitals of  $\text{Sr}_2\text{RuO}_4$  are decoupled to each other, and thus the calculation of the mirror topological numbers is simplified.

First, we calculate the mirror Chern number. Among the three orbitals of  $\text{Sr}_2\text{RuO}_4$ , only the  $d_{xy}$  orbital contributes to the mirror Chern number since other two orbitals reduce to be one-dimensional in the absence of the inter-orbit

coupling. The BdG Hamiltonian of the  $d_{xy}$  orbital is given by

$$\mathcal{H}_3 = \frac{1}{2} \sum_{\mathbf{k}ss'} (c_{\mathbf{k}s3}^\dagger, c_{-\mathbf{k}s3}) \begin{pmatrix} \varepsilon_{\mathbf{k}3} - \mu_B H_z \sigma_z & \hat{\Delta}^3(\mathbf{k}) \\ \hat{\Delta}^{3\dagger}(\mathbf{k}) & -\varepsilon_{-\mathbf{k}3} + \mu_B H_z \sigma_z \end{pmatrix}_{ss'} \begin{pmatrix} c_{\mathbf{k}s'3} \\ c_{-\mathbf{k}s'3}^\dagger \end{pmatrix}. \quad (\text{S.3})$$

To calculate the mirror Chern number, we block diagonalize the above Hamiltonian of the  $d_{xy}$  orbital in the diagonal basis of  $\tilde{\mathcal{M}}_{xy}$ . Each sector of the block diagonal Hamiltonian is a  $2 \times 2$  matrix with the following form,

$$\mathcal{H}_\lambda(\mathbf{k}) = \sum_{\mu=0}^3 h_{\mu;\lambda}(\mathbf{k}) \sigma_\mu, \quad (\text{S.4})$$

where  $\sigma_\mu = (\mathbf{1}, \sigma_a)$  ( $a = 1, 2, 3$ ) is the 4-component Pauli matrix, and  $\lambda$  denotes the eigenvalue of  $\tilde{\mathcal{M}}_{xy}$ . For the  $2 \times 2$  Hamiltonian, the mirror Chern number  $\nu(\lambda)$  is recast into

$$\nu(\lambda) = \frac{1}{8\pi} \int_{-\pi}^{\pi} \int_{-\pi}^{\pi} dk_x dk_y \epsilon^{ij} \epsilon^{abc} \hat{h}_{a;\lambda}(\mathbf{k}) \partial_{k_i} \hat{h}_{b;\lambda}(\mathbf{k}) \partial_{k_j} \hat{h}_{c;\lambda}(\mathbf{k}), \quad (\text{S.5})$$

with  $\hat{h}_{a;\lambda} = h_{a;\lambda} / \sqrt{\sum_{b=1}^3 h_{b;\lambda}^2}$ . Here the summations for  $i, j = x, y$  and  $a, b, c = 1, 2, 3$  are implicit. The last equation is evaluated as [1]

$$\nu(\lambda) = \frac{1}{2} \sum_{h_{1;\lambda}(\mathbf{k})=h_{2;\lambda}(\mathbf{k})=0} \text{sgn}[h_{3;\lambda}(\mathbf{k})] \text{sgn}[\det \partial_{k_i} h_{j;\lambda}(\mathbf{k})], \quad (\text{S.6})$$

where the summation is taken for  $\mathbf{k}$  satisfying  $h_{1;\lambda}(\mathbf{k}) = h_{2;\lambda}(\mathbf{k}) = 0$ , and

$$\det \partial_{k_i} h_{j;\lambda}(\mathbf{k}) = \det \begin{pmatrix} \partial_{k_x} h_{1;\lambda}(\mathbf{k}) & \partial_{k_x} h_{2;\lambda}(\mathbf{k}) \\ \partial_{k_y} h_{1;\lambda}(\mathbf{k}) & \partial_{k_y} h_{2;\lambda}(\mathbf{k}) \end{pmatrix}. \quad (\text{S.7})$$

This formula leads to the results summarized in Table I.

Now calculate the mirror  $\mathbf{Z}_2$  invariants for mirror even gap functions. By using the technique developed in Ref.[7], it is found that the mirror  $\mathbf{Z}_2$  invariant is directly related to the Fermi surface as

$$(-1)^{\nu_x(\lambda)} = \prod_l \text{sgn} \varepsilon_{\mathbf{k}=(\pi,0)l} \text{sgn} \varepsilon_{\mathbf{k}=(\pi,\pi)l}, \quad (-1)^{\nu_y(\lambda)} = \prod_l \text{sgn} \varepsilon_{\mathbf{k}=(0,\pi)l} \text{sgn} \varepsilon_{\mathbf{k}=(\pi,\pi)l}, \quad (\text{S.8})$$

which yields the results in Table I.

### S3. Model of edge dislocations

We explain our model for edge dislocations used in the calculation of Figs. 2 (c) and (d). As illustrated in Fig. S1, we place two edge dislocations with the Burgers vector  $\mathbf{B} = \pm \hat{e}_x$  and diagonalize the Hamiltonian Eq.(8) in the coordinate space. In actual calculation, we have used  $30 \times 30$  unit cell system with the periodic boundary condition and the two dislocations are separated by 15 unit length. Figures 2 (c) and (d) show the resultant eigen energies.

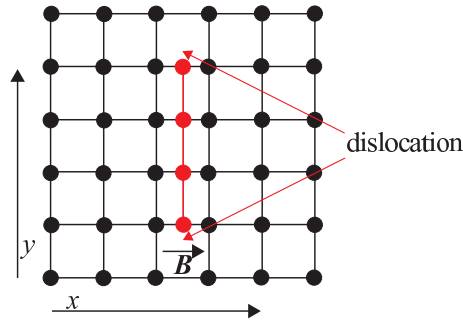


FIG. S1: Model of edge dislocations. Additional links are inserted to create edge dislocation with the Burgers vector  $\mathbf{B} = \pm \hat{e}_x$ .

While we have assumed that the parameters of the Hamiltonian near the dislocations are the same as those in the bulk, for simplicity, our result does not depend on the details: In Fig.S2, we show the quasiparticle spectra of a deformed edge dislocation where the double links near the dislocation in Fig.S2 (c) take different model parameters than those in the bulk. Figures S2 (a) and (b) clearly indicate that the qualitative behaviors are the same as those in Figs. 2(c) and (d), respectively.

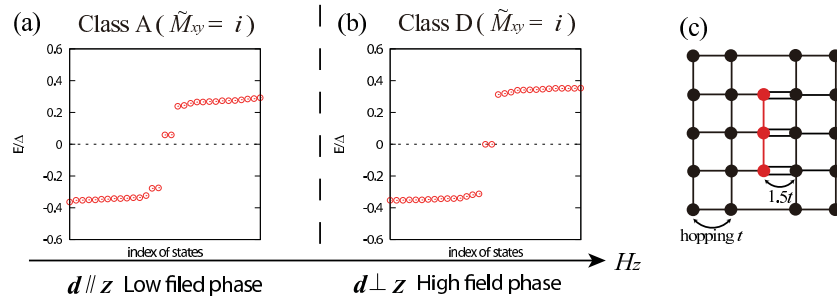


FIG. S2: (a) and (b) Bound states of the edge dislocations with deformed model parameters near the dislocations. The  $\mathbf{d}$ -vector is chosen as  $\mathbf{d}(\mathbf{k}) = \hat{z}(\sin k_x + i \sin k_y)$  in the low-field phase and as  $\mathbf{d}(\mathbf{k}) = \hat{x} \sin k_y - \hat{y} \sin k_x$  in the high-field phase. (c) Deformed edge dislocations. On the double lines in Fig.S2(c), we take  $t_1 = t_2 = 0.75$ ,  $t_3 = 0.3$ ,  $t_4 = 0.15$  and  $\Delta^l = 0.9$ . In other regions, the model parameters are the same as those used in Fig. 2.

#### S4. Robustness of mirror topological phase in $\text{Sr}_2\text{RuO}_4$

In this letter, we have assumed conventional chiral  $p$ -wave gap function in the low field phase of  $\text{Sr}_2\text{RuO}_4$ . However, our qualitative results rarely depend on the details of the gap function as far as the gap function is spin-triplet and the orientation of the  $\mathbf{d}$ -vector is the same: Since the parity of the gap function under the mirror reflection is the same as far as the orientation of the  $\mathbf{d}$ -vector is the same, as we pointed out in Sec.S1, the topological class of the mirror subsectors is also the same. Furthermore, for spin-triplet gap functions, one can show that the mirror  $\mathbf{Z}_2$  invariant (for  $\mathbf{d} \perp \hat{z}$ ) and the parity of the mirror Chern number are the same as far as the Fermi surface topology in the

normal state is the same [7]. This means that the mirror topological numbers are non-trivial, irrespectively of details of the gap function for  $\text{Sr}_2\text{RuO}_4$ .

For comparison, Figs. S3 (a) and (b) show the edge state and the bound state of the edge dislocation, respectively. The gap function is taken to be a recent proposed one in the low field phase [72],

$$\hat{\Delta}^l(\mathbf{k}) = i\Delta^l \mathbf{d}^l(\mathbf{k}) \cdot \boldsymbol{\sigma} \sigma_y, \quad (\text{S.9})$$

with

$$\mathbf{d}^1(\mathbf{k}) = i \sin k_y \cos k_x \hat{z}, \quad \mathbf{d}^2(\mathbf{k}) = \sin k_x \cos k_y \hat{z}, \quad \mathbf{d}^3(\mathbf{k}) = (\sin k_x + i \sin k_y) \hat{z}. \quad (\text{S.10})$$

These spectra are indeed qualitatively the same as those in Figs. 2 (a) and (c).

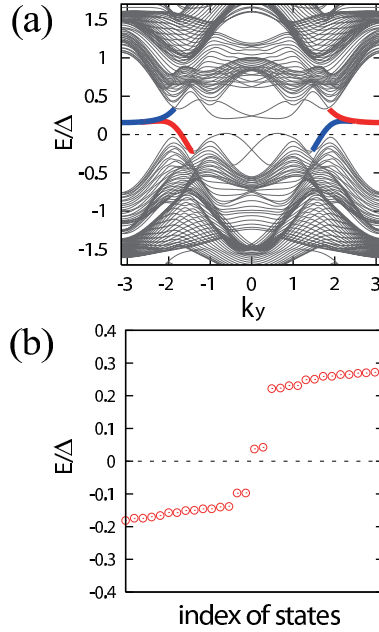


FIG. S3: Topological gapless states for the gap function Eqs.(S.9) and (S.10). (a) Edge state and (b) bound state of the edge dislocation. In (a), the red (blue) lines represent edge states localized at  $x = 0$  ( $x = L$ ). The model parameters are the same as those of Fig.2.

Our consideration also suggests that the gapless state in Fig. 2(b) can be gapful if one breaks the mirror symmetry with respect to the  $xy$ -plane. This is indeed the case as is illustrated in Fig.S4.

### S5. Effects of the spin-orbit interaction on edge modes in $\text{Sr}_2\text{RuO}_4$ .

While edge modes of  $\text{Sr}_2\text{RuO}_4$  have been studied intensively[43-49], the spin-orbit interaction had been ignored except for a recent work by Imai et al. [49], where the spin-orbit interaction was taken into account partially for the  $\alpha$  and

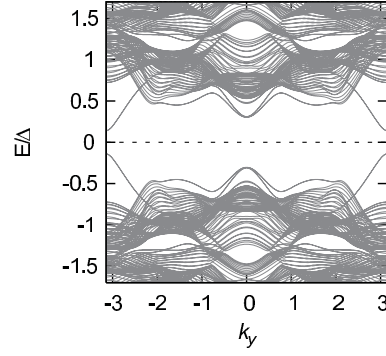


FIG. S4: Edge state in Fig.2 (b) under a magnetic field along the  $y$ -direction which breaks the mirror symmetry with respect to the  $xy$ -plane. Here we show the quasiparticle spectrum of the total system, not that in a mirror subsector, since the mirror symmetry is broken. We take  $\mu_B H_y = 0.1$  and  $\mu_B H_z = 0$ . Other model parameters are the same as those of Fig.2 (b).

$\beta$ -bands. In the present letter, we consider the spin-orbit interaction for full three  $\alpha$ ,  $\beta$  and  $\gamma$ -bands in  $\text{Sr}_2\text{RuO}_4$ . Here we illustrate that the edge mode spectra are considerably affected by the spin-orbit interaction.

In Figs. S5 (a)-(d), we compare the edge state spectra with and without the spin-orbit interaction. To sharpen the effect of the spin-orbit interaction, we set the magnetic field  $H_z$  as zero in the numerical calculations in Fig. S5, but other model parameters are the same as those in Fig. 2. It is found that the edge state spectra are fairly changed by the spin-orbit interaction. In particular, Fig. S5 clearly indicates that the degeneracy of the edge modes at  $k_y = 0$  reported in Refs.[43-47,49] is resolved by the spin-orbit interaction.

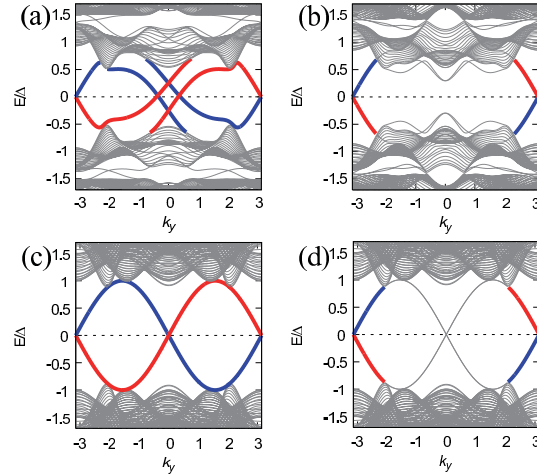


FIG. S5: Edge states with [(a) and (b)] and without [(c) and (d)] the spin-orbit interaction. The  $\mathbf{d}$ -vector is chosen as  $\mathbf{d}(\mathbf{k}) = \hat{\mathbf{z}}(\sin k_x + i \sin k_y)$  in (a) and (c), and  $\mathbf{d}(\mathbf{k}) = \hat{\mathbf{x}} \sin k_y - \hat{\mathbf{y}} \sin k_x$  in (b) and (d). In (c) and (d), the gapless edge modes around  $k_y = 0$  are two-fold degenerate. The red (blue) lines represent edge states localized at  $x = 0$  ( $x = L$ ). [Around  $k_y = 0$  in (d), a pair of left and right moving edge modes are localized on each edge.] We take  $\mu_B H_z = 0$ ,  $\lambda = 0.3$  in (a) and (b), and  $\lambda = 0$  in (c) and (d), respectively. Other model parameters are the same as those of Figs.2 (a) and (b).

---

\* Electronic address: [msato@nuap.nagoya-u.ac.jp](mailto:msato@nuap.nagoya-u.ac.jp)  
[72] S. Raghu, K. Kapitulnik and S. A. Kivelson, *Phys. Rev. Lett.* **105**, 136401 (2010).